Supplementary information

Tuning Covalent Bonding in Znic-Based Hybrid Halides towards Tunable Room-Temperature Phosphorescence

Yibo Cui,[a] Jiawei Lin,[b] Kunjie Liu,[a] Yuhe Shao,[a] Dong Zhao,[a] Zhongnan Guo,[b] Jing Zhao,*[a] Zhiguo Xia*[c] and Quanlin Liu*[a]

a. The Beijing Municipal Key Laboratory of New Energy Materials and Technologies, School of Materials Science and Engineering, University of Science and Technology Beijing, Beijing 100083, P. R. China

b. The Beijing Municipal Key Laboratory of New Energy Materials and Technologies, School of Materials Sciences and Engineering and Chemistry and Biological Engineering, University of Science and Technology Beijing, Beijing 100083, China.

c. State Key Laboratory of Luminescent Materials and Devices, Guangdong Provincial Key Laboratory of Fiber Laser Materials and Applied Techniques, Guangdong Engineering Technology Research and Development Centre of Special Optical Fiber Materials and Devices, School of Physics and Optoelectronics, South China University of Technology, Guangzhou, 510641 China

*Corresponding author E-mail: Jing Zhao: jingzhao@ustb.edu.cn; Zhiguo Xia: xiazg@scut.edu.cn; Quanlin Liu: qlliu@ustb.edu.cn.

Contents

1. Figures

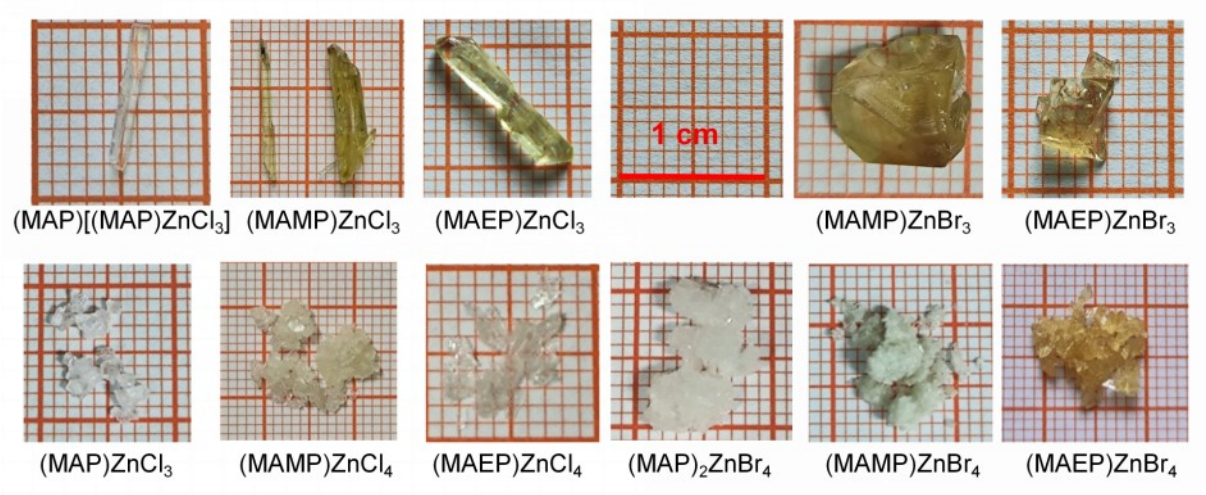

Figure S1. Optical images of newly synthesized compound crystals.

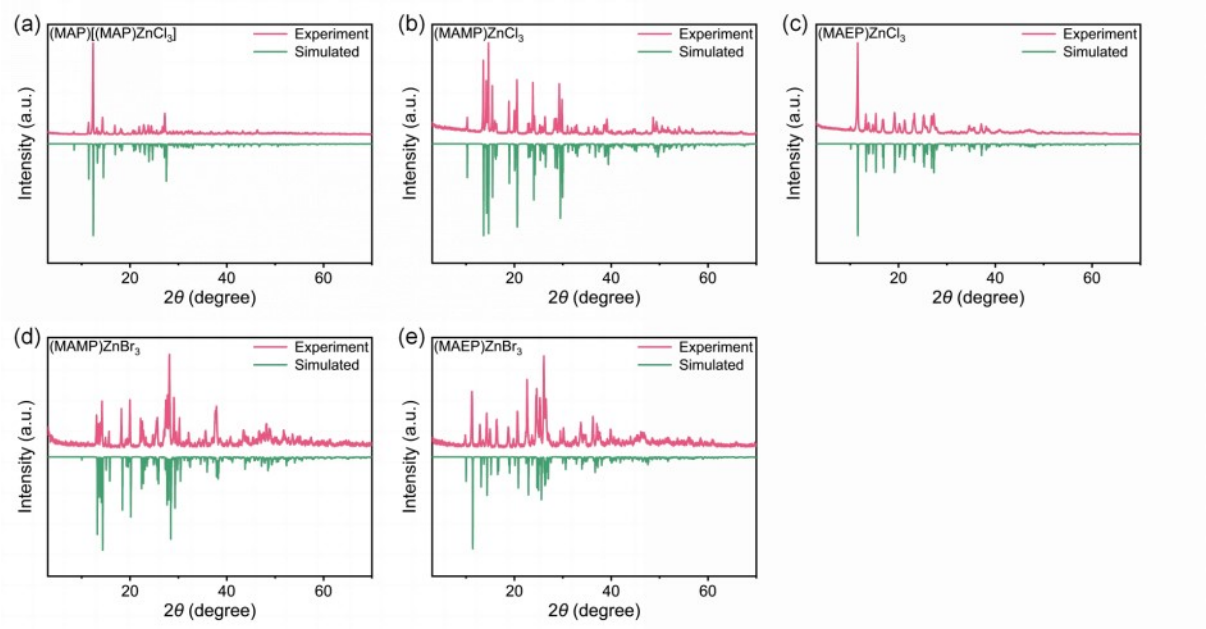

Figure S2. Comparison of simulated and experimental powder XRD patterns for the Type-*C* series compounds.

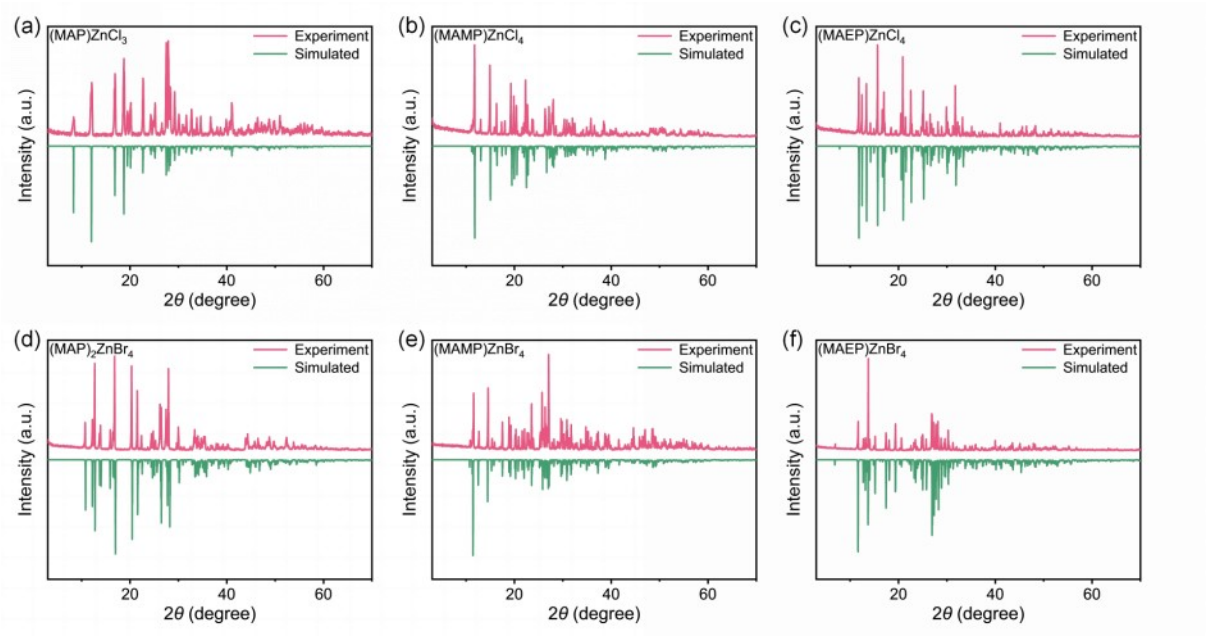

Figure S3. Comparison of simulated and experimental powder XRD patterns for the Type-*H* series compounds.

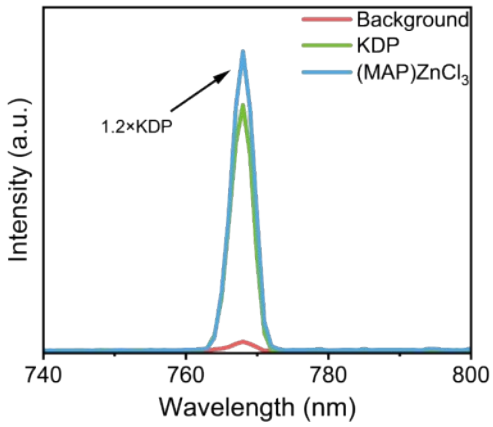

Figure S4. SHG testing for $(MAP)ZnCl_3$.

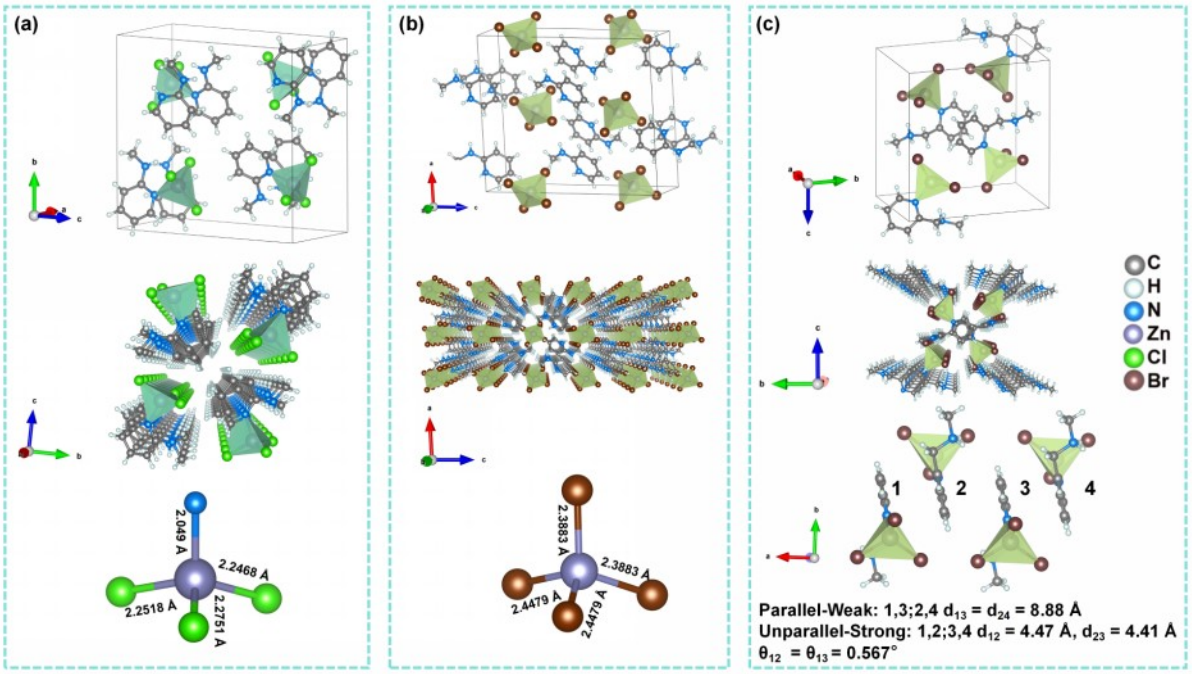

Figure S5. (a) Crystal structure of (MAP)[(MAP)$ZnCl_3$], (b) (MAMP)$ZnBr_4$, and (c) (MAMP)$ZnBr_3$.

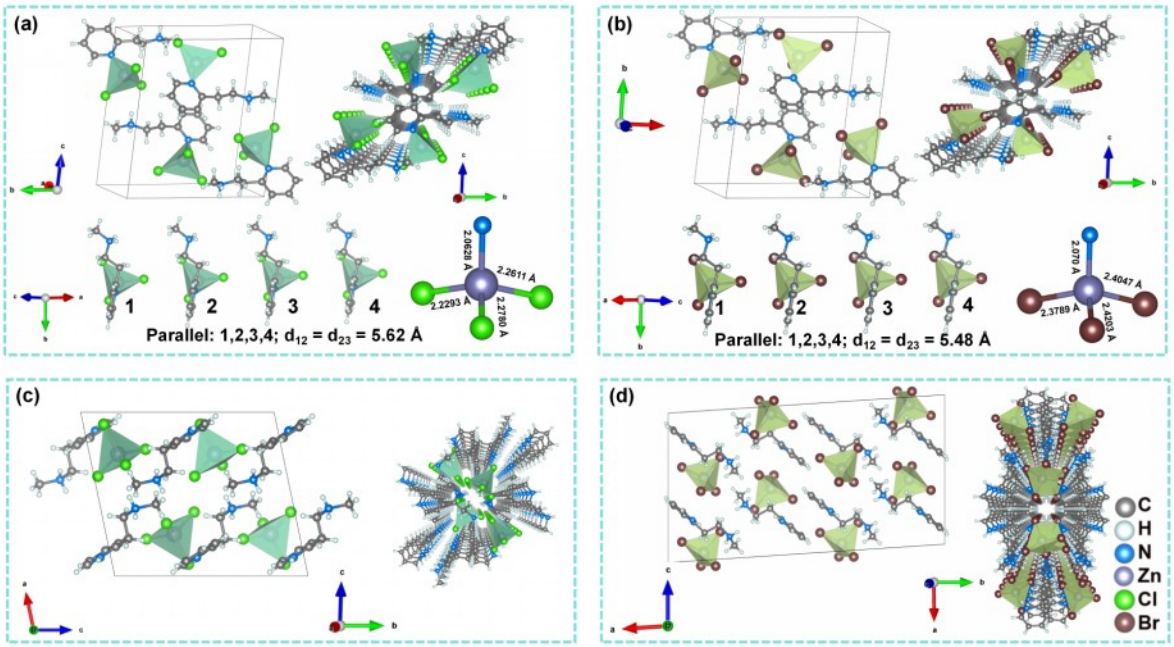

Figure S6. (a) Crystal structure of (MAEP)$ZnCl_3$, (b) (MAEP)$ZnBr_3$, (c) (MAEP)$ZnCl_4$, and (d) (MAEP)$ZnBr_4$.

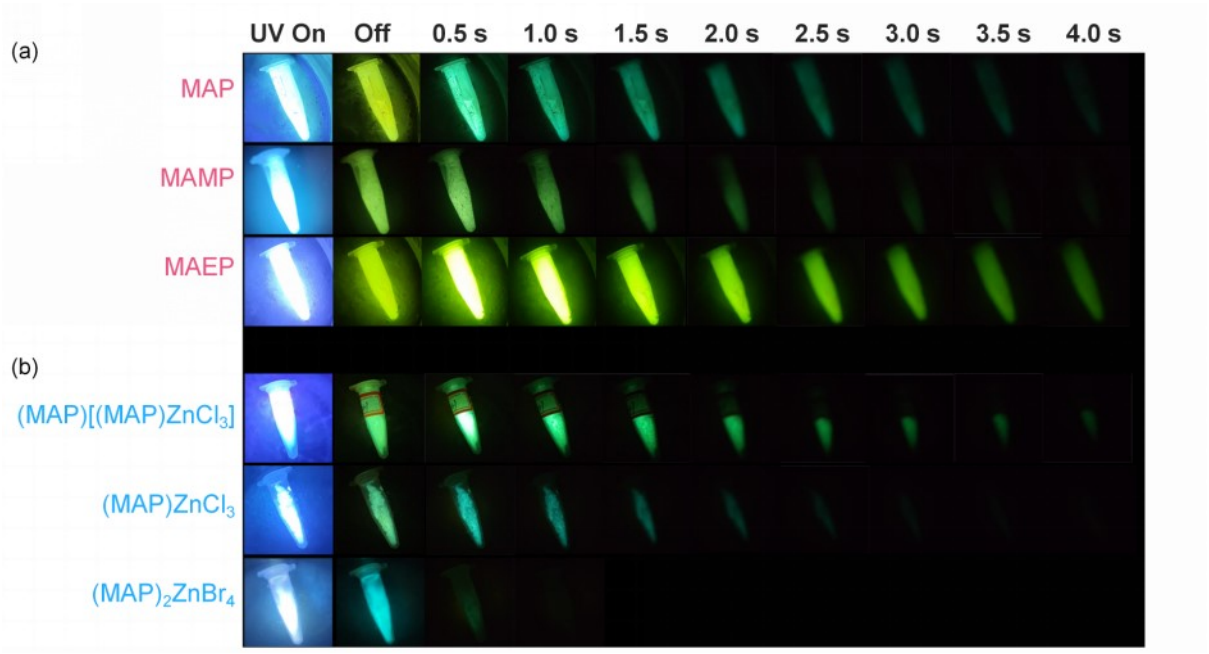

Figure S7.(a) Photographs of the luminescence of MAP, MAMP, and MAEP compounds before and after exposure to 365 nm UV light at 80 K. (b) Photographs of the luminescence of MAP-based compounds before and after exposure to 365 nm UV light at 80 K.

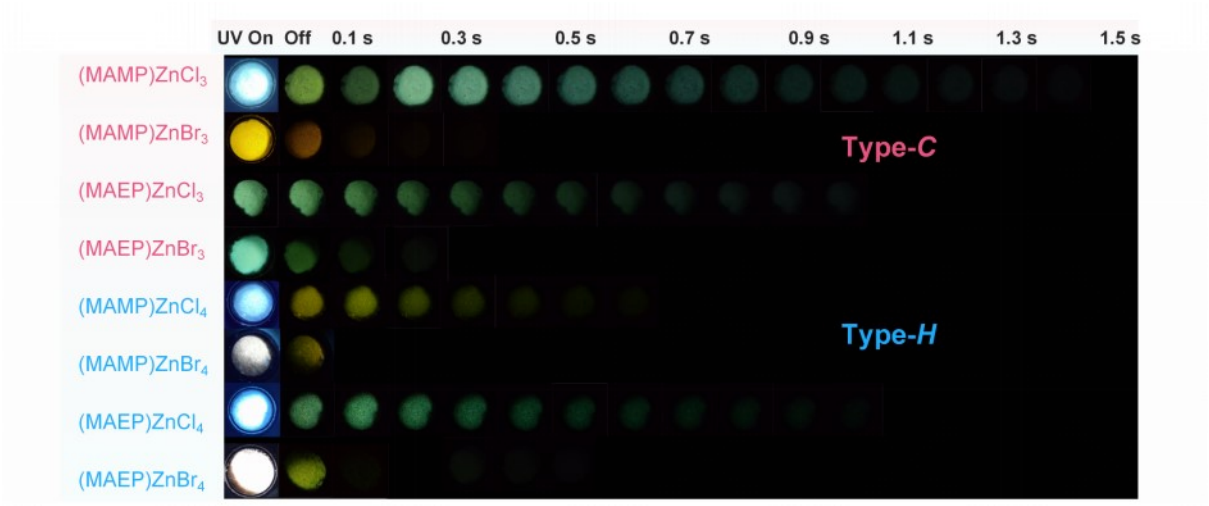

Figure S8. Photographs of the luminescence of MAMP and MAEP-based compounds in powder form before and after exposure to 365 nm UV light.

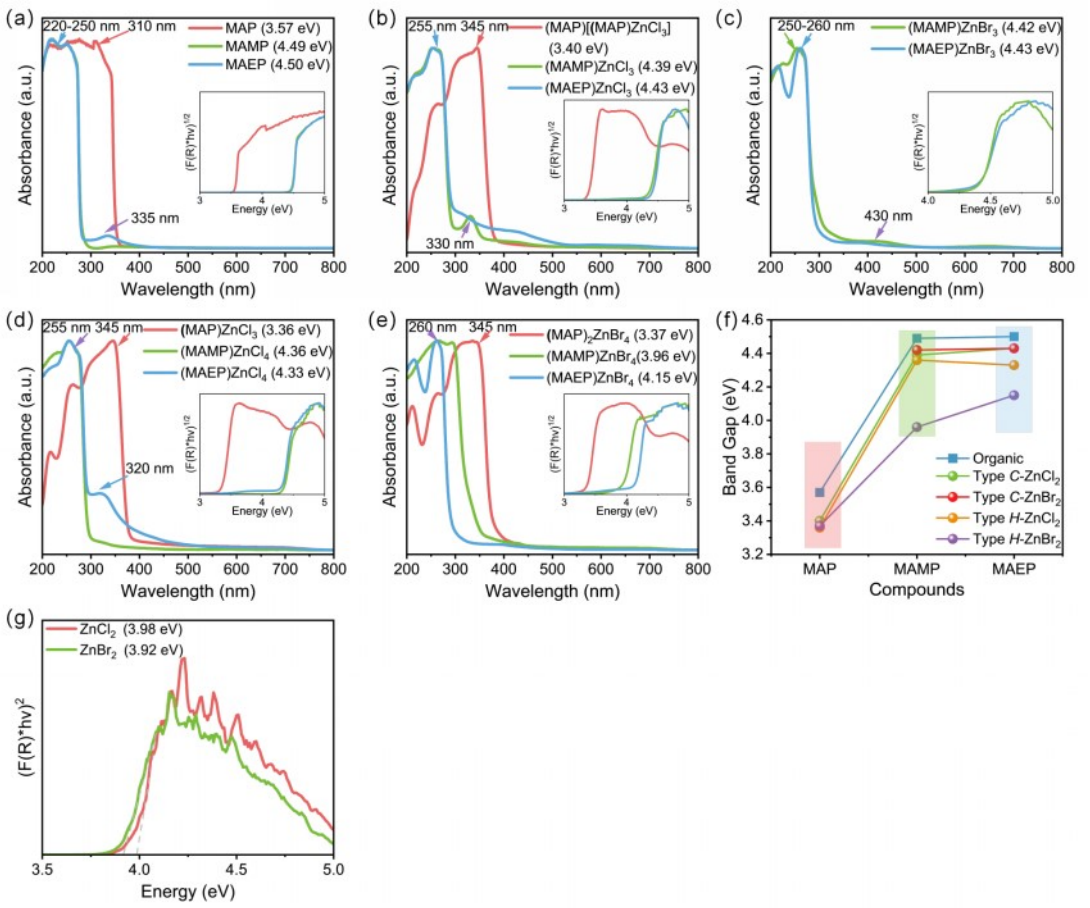

Figure S9. UV-visible diffuse reflectance spectra and corresponding optical bandgaps of the synthesized series of compounds, organic materials, and inorganic materials.

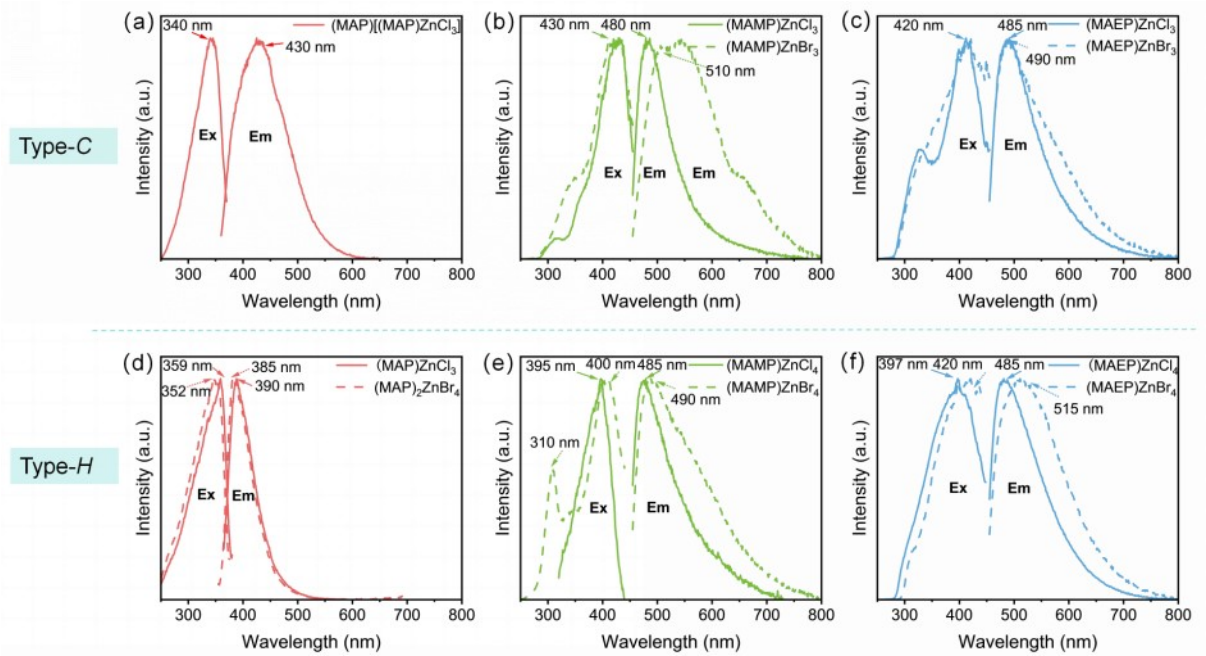

Figure S10. PL and PLE spectra of the synthesized series of compounds and organic materials.

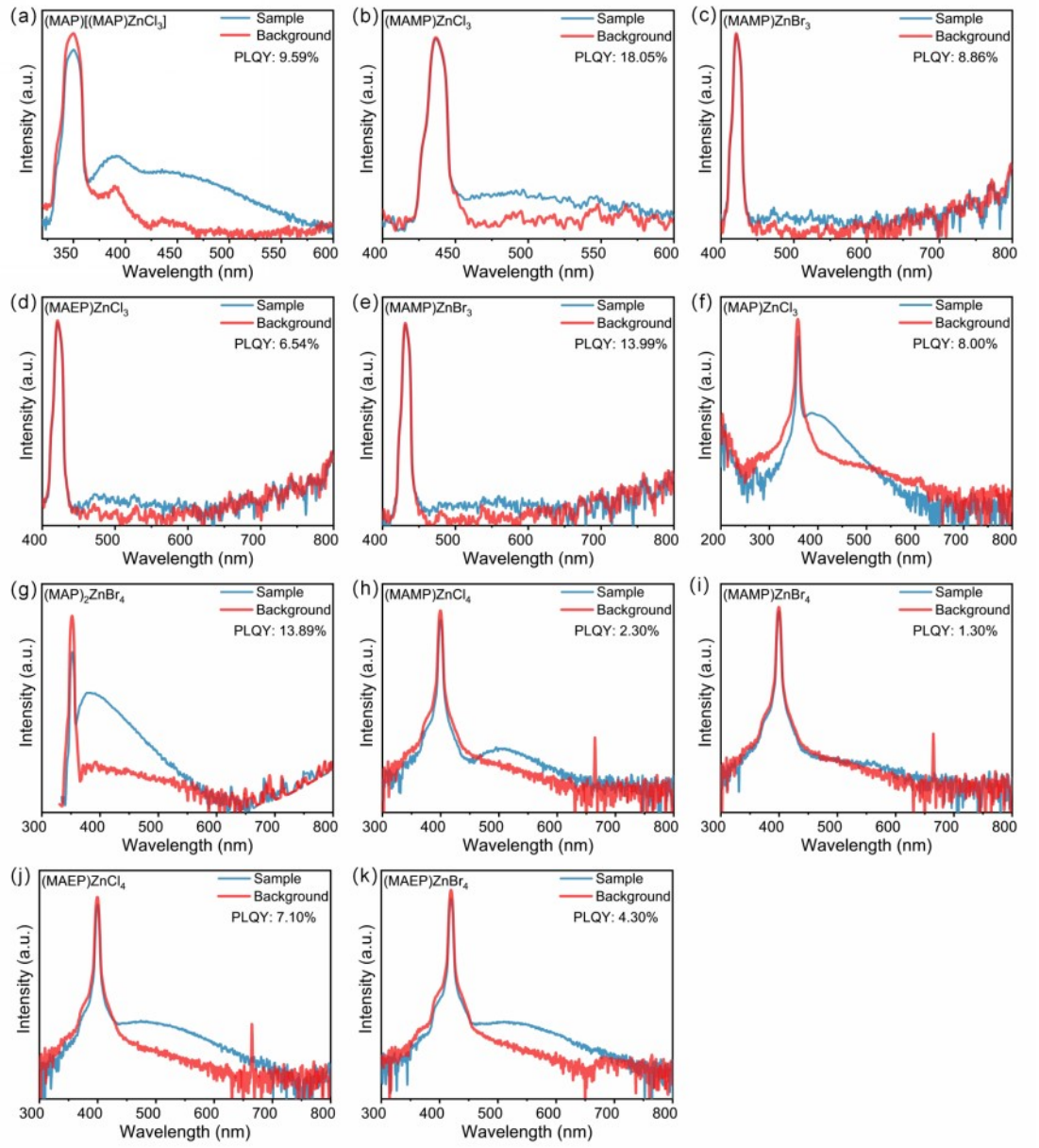

Figure S11. The PLQY of all the 11 compounds.

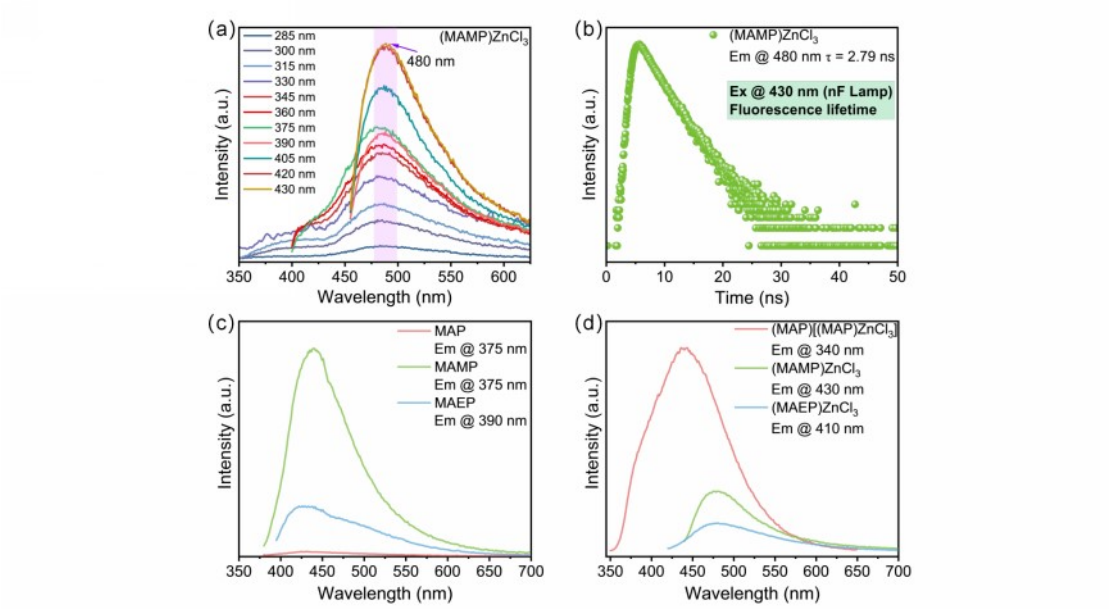

Figure S12. (a) Emission spectra of (MAMP)$ZnCl_3$ under different excitation wavelengths, (b) Fluorescence lifetime of (MAMP)$ZnCl_3$ monitored at 480 nm under 430 nm excitation, (c) Comparison of emission intensities for MAP, MAMP, and MAEP, (d) Comparison of emission intensities for (MAP)[(MAP)$ZnCl_3$], (MAMP)$ZnCl_3$, and (MAEP)$ZnCl_3$.

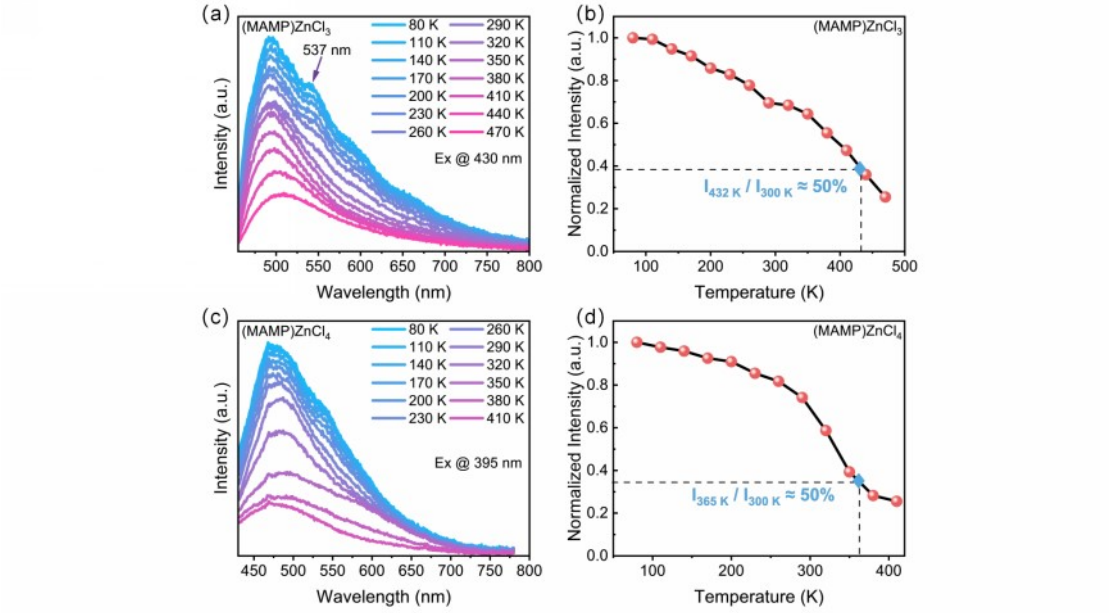

Figure S13. (a) and (c) Temperature-dependent PL spectra. (b) and (d) PL intensity variation as a function of temperature.

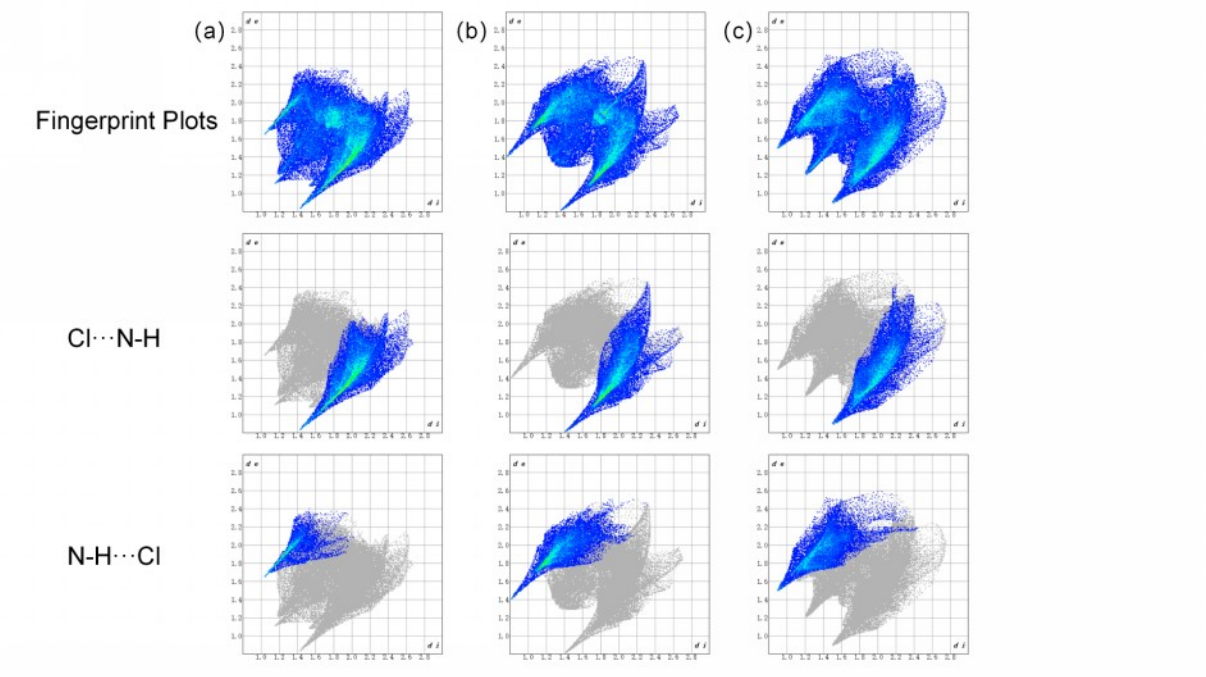

Figure S14. (a) Fingerprint plot of (MAP)[(MAP)$ZnCl_3$], (b) (MAMP)$ZnCl_3$, and (c) (MAEP)$ZnCl_3$, illustrating all intermolecular interactions. Specific contributions of Cl···N-H and N-H···Cl interactions are highlighted.

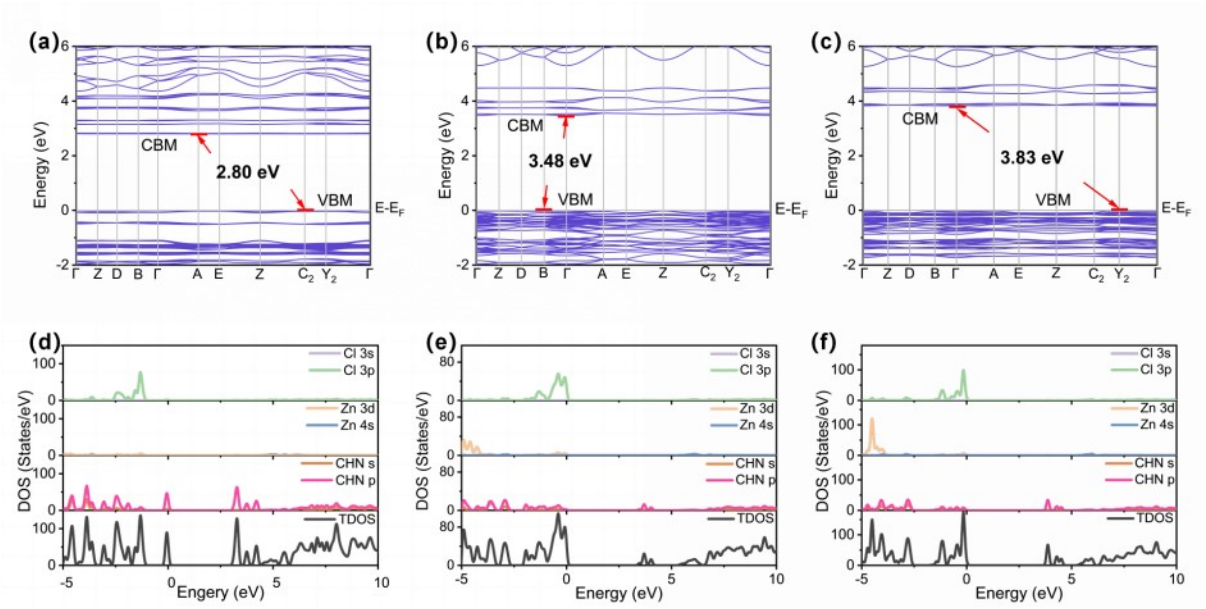

Figure S15. DFT calculated band gaps and DOS distribution for (a), (d) (MAP)[(MAP)$ZnCl_3$]; (b), (e) (MAMP)$ZnCl_3$; (c), (f) (MAEP)$ZnCl_3$.

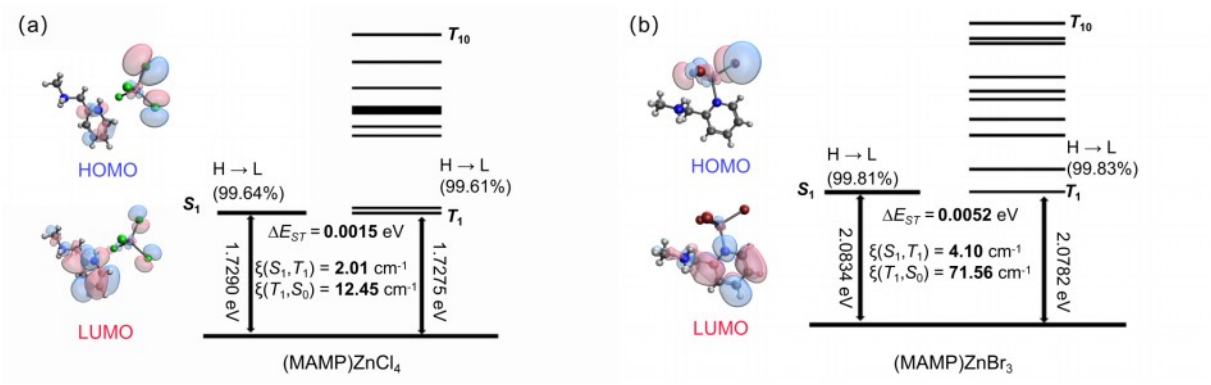

Figure S16. The TD-DFT-calculated SOC coefficients and energy level diagrams for the compounds (a) (MAMP)$ZnCl_4$ and (b) (MAMP)$ZnBr_3$ are presented. Insets show the charge distributions of the LUMO and HOMO orbitals.

2. Tables

Table S1. Structural Parameters of All Compounds.

Compound	Bonding Mechanisms	Space group	Bond length distortion (λ)	Bond angle distortion (σ^2)	d_{min} (Metal-Metal) Å
$(MAP)ZnCl_3$	Type-*H*	*Cc*	6.36×10^{-4}	21.81	3.99
$(MAP)_2ZnBr_4$		*C*2/*c*	1.52×10^{-4}	12.59	7.89
$(MAMP)ZnCl_4$		$P2_1/n$	4.73×10^{-5}	7.47	5.50
$(MAMP)ZnBr_4$		$P2_1/n$	4.49×10^{-5}	6.86	5.65
$(MAEP)ZnCl_4$		$P2_1/c$	9.77×10^{-5}	11.83	6.64
$(MAEP)ZnBr_4$		*C*2/*c*	4.49×10^{-4}	19.78	6.93
$(MAPH)[(MAP)ZnCl_3]$	Type-*C*	$P2_1/n$	1.71×10^{-3}	7.62	7.45
$(MAMP)ZnCl_3$		$P2_1/n$	1.17×10^{-3}	18.22	6.13
$(MAMP)ZnBr_3$		$P2_1/n$	3.19×10^{-3}	19.44	6.27
$(MAEP)ZnCl_3$		$P2_1/n$	1.50×10^{-3}	19.54	5.91
$(MAEP)ZnBr_3$		$P2_1/n$	3.87×10^{-3}	18.99	5.98

The distortion of the octahedron in the OIMHs was characterized using the following equations, which are:

$$\lambda = (\frac{1}{4})\sum_{n=1}^{4}(\frac{d_n - d}{d})^2 \quad (2)$$

$$\sigma^2 = \left(\frac{1}{5}\right)\sum_{i=1}^{6}\left(\theta_i - 109.4^{\circ}\right)^2, \quad (3)$$

where d_n are the Zn–Cl, Zn-Br and Zn-N bond lengths, d is the average bond length, and θ_i is the bond angle.[1]

Table S2. Crystal data and structure refinement for $(MAP)ZnCl_3$, $(MAP)[(MAP)ZnCl_3]$ and $(MAP)_2ZnBr_4$ at 150.0 K.

Empirical formula	$(MAP)ZnCl_3$	$(MAP)[(MAP)ZnCl_3]$	$(MAP)_2ZnBr_4$
Formula weight	281.32	389.01	603.31
Temperature	150.15 K	150.0 K	150.0 K
Wavelength	0.71073 Å	0.71073 Å	0.71073 Å
Crystal system	Monoclinic	Monoclinic	Monoclinic
Space group	*Cc*	$P2_1/n$	$C2/c$
Unit cell dimensions	*a* = 9.909(2) Å, *b* = 63.672(16) Å, *c* = 6.3765(15) Å, *β* = 127.717(7)°	*a* = 7.4537(4) Å, *b* = 14.2418(7) Å, *c* = 15.4069(6) Å, *β* = 91.025(2)°	*a* = 14.4961(6) Å, *b* = 7.8886(4) Å, *c* = 16.3790(8) Å, *β* = 93.194(2)°
Volume	3182.5(14) $Å^3$	1635.24(13) $Å^3$	1870.09(15) $Å^3$
Z	12	4	4
Density (calculated)	1.761 g/cm^3	1.580 g/cm^3	2.143 g/cm^3
Absorption coefficient	3.032 mm^{-1}	1.986 mm^{-1}	9.858 mm^{-1}
F(000)	1683	792	1152
θ range for data collection	2.559 to 30.590°	3.007 to 26.509°	2.491 to 26.412°
Index ranges	-14≤*h*≤13, -90≤*k*≤90, -9≤*l*≤9	-9≤*h*≤9, -17≤*k*≤17, -17≤*l*≤19	-18≤*h*≤18, -9≤*k*≤9, -20≤*l*≤20
Reflections collected	38851	28796	13958
Independent reflections	9345 [R_{int} = 0.0563]	3368 [R_{int} = 0.0610]	1926 [R_{int} = 0.0367]
Completeness to *θ* = 25.242°	99.8%	99.7%	100%
Refinement method	Full-matrix least-squares on F^2	Full-matrix least-squares on F^2	Full-matrix least-squares on F^2
Data / restraints / parameters	9345 / 116 / 310	3368 / 0 / 183	1926 / 0 / 97
Goodness-of-fit	1.019	1.123	1.038
Final *R* indices [$I > 2\sigma(I)$]	R_{obs} = 0.0546, wR_{obs} = 0.1048	R_{obs} = 0.0384, wR_{obs} = 0.0889	R_{obs} = 0.0219, wR_{obs} = 0.0496
R indices [all data]	R_{all} = 0.1208, wR_{all} = 0.1348	R_{all} = 0.0484, wR_{all} = 0.0949	R_{all} = 0.0324, wR_{all} = 0.0533
Largest diff. peak and hole	1.186 and -0.874 e·$Å^{-3}$	0.404 and -0.463 e·$Å^{-3}$	0.348 and -0.417 e·$Å^{-3}$

For $(MAP)ZnCl_3$, $R = \Sigma||F_o|-|F_c|| / \Sigma|F_o|$, $wR = \{\Sigma[w(|F_o|^2 - |F_c|^2)^2] / \Sigma[w(|F_o|^4)]\}^{1/2}$ and $w=1/[\sigma^2(F_o^2)+(0.0418P)^2+13.6228P]$ where $P=(F_o^2+2F_c^2)/3$;

For $(MAP)[(MAP)ZnCl_3]$, $R = \Sigma||F_o|-|F_c|| / \Sigma|F_o|$, $wR = \{\Sigma[w(|F_o|^2 - |F_c|^2)^2] / \Sigma[w(|F_o|^4)]\}^{1/2}$ and $w=1/[\sigma^2(F_o^2)+(0.0422P)^2+1.0732P]$ where $P=(F_o^2+2F_c^2)/3$;

For $(MAP)_2ZnBr_4$, $R = \Sigma||F_o|-|F_c|| / \Sigma|F_o|$, $wR = \{\Sigma[w(|F_o|^2 - |F_c|^2)^2] / \Sigma[w(|F_o|^4)]\}^{1/2}$ and $w=1/[\sigma^2(F_o^2)+(0.0287P)^2+0.1102P]$ where $P=(F_o^2+2F_c^2)/3$;

Table S3. Crystal data and structure refinement for $(MAMP)ZnCl_3$, $(MAMP)ZnCl_4$, $(MAMP)ZnBr_3$ and $(MAMP)ZnBr_4$ at 150.0 K.

Empirical formula	$(MAMP)ZnCl_3$	$(MAMP)ZnCl_4$	$(MAMP)ZnBr_3$	$(MAMP)ZnBr_4$
Formula weight	294.90	331.36	428.28	509.20
Temperature	150.0 K	150.0 K	150.0 K	150.0 K
Wavelength	0.71073 Å	0.71073 Å	0.71073 Å	0.71073 Å
Crystal system	Monoclinic	Monoclinic	Monoclinic	Monoclinic
Space group	$P2_1/n$	$P2_1/n$	$P2_1/n$	$P2_1/n$
Unit cell dimensions	a = 7.4173(2) Å, b = 12.0708(4) Å, c = 12.3184(3) Å, β = 92.933(1)°	a = 9.3199(4) Å, b = 13.5559(6) Å, c = 10.0752(4) Å, β = 105.093(2)°	a = 7.7054(2) Å, b = 12.3265(3) Å, c = 12.5814(3) Å, β = 92.110(1)°	a = 9.5132(5) Å, b = 14.1340(6) Å, c = 10.4282(4) Å, β = 104.052(1)°
Volume	1101.46(5) $Å^3$	1228.99(9) $Å^3$	1194.18(5) $Å^3$	1360.21(11) $Å^3$
Z	4	4	4	4
Density (calculated)	1.778 g/cm^3	1.791 g/cm^3	2.382 g/cm^3	2.486 g/cm^3
Absorption coefficient	2.913 mm^{-1}	2.831 mm^{-1}	12.054 mm^{-1}	13.524 mm^{-1}
$F(000)$	592	664	808	952
θ range for data collection	2.364 to 26.431°	2.577 to 26.444°	2.31 to 26.44°	2.476 to 26.486°
Index ranges	-9<=h<=9, -15<=k<=15, -15<=l<=15	-11<=h<=11, -16<=k<=16, -12<=l<=12	-9<=h<=9, -15<=k<=15, -15<=l<=15	-11<=h<=11, -17<=k<=17, -13<=l<=13
Reflections collected	19581	18659	25754	29232
Independent reflections	2260 [R_{int} = 0.0291]	2522 [R_{int} = 0.0343]	2457 [R_{int} = 0.0507]	2797 [R_{int} = 0.0831]
Completeness to θ = 25.242°	99.9%	100%	99.7%	100%
Refinement method	Full-matrix least-squares on F^2	Full-matrix least-squares on F^2	Full-matrix least-squares on F^2	Full-matrix least-squares on F^2
Data / restraints / parameters	2260 / 0 / 119	2522 / 0 / 128	2457 / 0 / 119	2797 / 0 / 128
Goodness-of-fit	1.078	1.053	1.067	1.002
Final R indices [$I > 2\sigma(I)$]	R_{obs} = 0.0218, wR_{obs} = 0.0505	R_{obs} = 0.0218, wR_{obs} = 0.0504	R_{obs} = 0.0243, wR_{obs} = 0.0497	R_{obs} = 0.0284, wR_{obs} = 0.0525
R indices [all	R_{all} = 0.0267,	R_{all} = 0.0301,	R_{all} = 0.0369,	R_{all} = 0.0508,

data]	wR_{all} = 0.0521	wR_{all} = 0.0533	wR_{all} = 0.0535	wR_{all} = 0.0588
Largest diff.	0.248 and -0.354	0.244 and -0.254	0.396 and -0.573	0.521 and -0.489
peak and hole	e·Å^{-3}	e·Å^{-3}	e·Å^{-3}	e·Å^{-3}

For $(MAMP)ZnCl_3$, $R = \Sigma||F_o|-|F_c|| / \Sigma|F_o|$, $wR = \{\Sigma[w(|F_o|^2 - |F_c|^2)^2] / \Sigma[w(|F_o|^4)]\}^{1/2}$ and $w=1/[\sigma^2(F_o^2)+(0.0260P)^2+0.4010P]$ where $P=(F_o^2+2F_c^2)/3$;

For $(MAMP)ZnCl_4$, $R = \Sigma||F_o|-|F_c|| / \Sigma|F_o|$, $wR = \{\Sigma[w(|F_o|^2 - |F_c|^2)^2] / \Sigma[w(|F_o|^4)]\}^{1/2}$ and $w=1/[\sigma^2(F_o^2)+(0.0266P)^2+0.3004P]$ where $P=(F_o^2+2F_c^2)/3$；

For $(MAMP)ZnBr_3$, $R = \Sigma||F_o|-|F_c|| / \Sigma|F_o|$, $wR = \{\Sigma[w(|F_o|^2 - |F_c|^2)^2] / \Sigma[w(|F_o|^4)]\}^{1/2}$ and $w=1/[\sigma^2(F_o^2)+(0.0257P)^2+0.2487P]$ where $P=(F_o^2+2F_c^2)/3$；

For $(MAMP)ZnBr_4$, $R = \Sigma||F_o|-|F_c|| / \Sigma|F_o|$, $wR = \{\Sigma[w(|F_o|^2 - |F_c|^2)^2] / \Sigma[w(|F_o|^4)]\}^{1/2}$ and $w=1/[\sigma^2(F_o^2)+(0.0255P)^2]$ where $P=(F_o^2+2F_c^2)/3$；

Table S4. Crystal data and structure refinement for $(MAEP)ZnCl_3$, $(MAEP)ZnCl_4$, $(MAEP)ZnBr_3$ and $(MAEP)ZnBr_4$ at 150.0 K.

Empirical formula	$(MAEP)ZnCl_3$	$(MAEP)ZnCl_4$	$(MAEP)ZnBr_3$	$(MAEP)ZnBr_4$
Formula weight	308.92	345.38	442.30	523.22
Temperature	150.15 K	150.0 K	150.0 K	150.0 K
Wavelength	0.71073 Å	0.71073 Å	0.71073 Å	0.71073 Å
Crystal system	Monoclinic	Monoclinic	Monoclinic	Monoclinic
Space group	$P2_1/n$	$P2_1/c$	$P2_1/n$	$C2/c$
Unit cell dimensions	a = 8.0104(2) Å, b = 11.5319(4) Å, c = 13.8196(4) Å, β = 105.6670(10)°	a = 11.5216(4) Å, b = 9.1377(3) Å, c = 13.3073(4) Å, β = 101.7470(10)°	a = 8.2015(3) Å, b = 11.6705(4) Å, c = 13.9617(4) Å, β = 104.9890(10)°	a = 25.8746(8) Å, b = 7.9515(3) Å, c = 13.9583(5) Å, β = 93.8010(10)°
Volume	1229.16(6) Å^3	1371.66(8) Å^3	1290.88(7) Å^3	2865.49(17) Å^3
Z	4	4	4	8
Density (calculated)	1.669 g/cm^3	1.672 g/cm^3	2.276 g/cm^3	2.426 g/cm^3
Absorption coefficient	2.614 mm^{-1}	2.541 mm^{-1}	11.155 mm^{-1}	12.842 mm^{-1}
F(000)	624	696	840	1968
θ range for data collection	2.337 to 26.373°	2.723 to 26.392°	2.308 to 26.386°	2.680 to 26.526°
Index ranges	-9<=h<=9, -14<=k<=14, -17<=l<=17	-14<=h<=14, -11<=k<=11, -16<=l<=16	-10<=h<=10, -14<=k<=14, -17<=l<=17	-32<=h<=32, -9<=k<=9, -17<=l<=17
Reflections collected	19209	25970	28293	27481
Independent reflections	2512 [R_{int} = 0.0450]	2815 [R_{int} = 0.0516]	2640 [R_{int} = 0.0571]	2948 [R_{int} = 0.0580]

Completeness to θ = 25.242°	100%	100%	99.7%	100%
Refinement method	Full-matrix least-squares on F^2	Full-matrix least-squares on F^2	Full-matrix least-squares on F^2	Full-matrix least-squares on F^2
Data / restraints / parameters	2512 / 0 / 128	2815 / 0 / 137	2640 / 0 / 128	2948 / 0 / 140
Goodness-of-fit	1.048	1.040	1.100	1.002
Final R indices [$I > 2\sigma(I)$]	R_{obs} = 0.0351, wR_{obs} = 0.0565	R_{obs} = 0.0248, wR_{obs} = 0.0517	R_{obs} = 0.0400, wR_{obs} = 0.1157	R_{obs} = 0.0240, wR_{obs} = 0.0489
R indices [all data]	R_{all} = 0.0650, wR_{all} = 0.0656	R_{all} = 0.0388, wR_{all} = 0.0560	R_{all} = 0.0466, wR_{all} = 0.1214	R_{all} = 0.0386, wR_{all} = 0.0532
Largest diff. peak and hole	0.290 and -0.291 e·Å^{-3}	0.289 and -0.241 e·Å^{-3}	1.113 and -1.254 e·Å^{-3}	0.351 and -0.408 e·Å^{-3}

For (MAEP)$ZnCl_3$, $R = \Sigma||F_o|-|F_c|| / \Sigma|F_o|$, w$R = \{\Sigma[w(|F_o|^2 - |F_c|^2)^2] / \Sigma[w(|F_o|^4)]\}^{1/2}$ and $w=1/[\sigma^2(F_o^2)+(0.0189P)^2+0.8980P]$ where $P=(F_o^2+2F_c^2)/3$;

For (MAEP)$ZnCl_4$, $R = \Sigma||F_o|-|F_c|| / \Sigma|F_o|$, w$R = \{\Sigma[w(|F_o|^2 - |F_c|^2)^2] / \Sigma[w(|F_o|^4)]\}^{1/2}$ and $w=1/[\sigma^2(F_o^2)+(0.0239P)^2+0.3522P]$ where $P=(F_o^2+2F_c^2)/3$；

For (MAEP)$ZnBr_3$, $R = \Sigma||F_o|-|F_c|| / \Sigma|F_o|$, w$R = \{\Sigma[w(|F_o|^2 - |F_c|^2)^2] / \Sigma[w(|F_o|^4)]\}^{1/2}$ and $w=1/[\sigma^2(F_o^2)+(0.0831P)^2+0.6475P]$ where $P=(F_o^2+2F_c^2)/3$；

For (MAEP)$ZnBr_4$, $R = \Sigma||F_o|-|F_c|| / \Sigma|F_o|$, w$R = \{\Sigma[w(|F_o|^2 - |F_c|^2)^2] / \Sigma[w(|F_o|^4)]\}^{1/2}$ and $w=1/[\sigma^2(F_o^2)+(0.0272P)^2]$ where $P=(F_o^2+2F_c^2)/3$；

Table S5. Proportional Contributions of Intermolecular Interactions in (MAP)[(MAP)$ZnCl_3$], (MAMP)$ZnCl_3$, and (MAEP)$ZnCl_3$.

Compound	H-X (%)	H-H (%)	H-C (%)	Other
(MAP)[(MAP)$ZnCl_3$]	49.3	32.9	11.5	6.3
(MAMP)$ZnCl_3$	58.3	25.8	4.7	11.2
(MAEP)$ZnCl_3$	58	26.1	10.1	5.8

Table S6. Natural transition orbitals (NTOs) for (MAP)[(MAP)$ZnCl_3$].

	n-th	Energy (eV)	Transition configuration (%)
S_n	1	1.9456	H → L (97.75)
	2	2.0404	H-1 → L (98.01)
	3	2.1778	H-2 → L (98.17)
	4	2.3192	H-3 → L (97.09)
	5	2.5430	H-4 → L (96.28)
	6	2.7646	H-5 → L (96.83)
	7	2.9362	H-7 → L (4.04), H-6 → L (93.28)
	8	3.0682	H → L+1 (97.87)
	9	3.1631	H-1 → L+1 (98.11)
	10	3.2667	H-7 → L (93.29), H-6 → L (3.93)
T_n	1	1.9434	H → L (97.65)
	2	2.0400	H-1 → L (97.97)
	3	2.1770	H-2 → L (98.09)
	4	2.3180	H-3 → L (97.01)
	5	2.5412	H-4 → L (95.89)
	6	2.7356	H-5 → L (95.21)
	7	2.9241	H-7 → L (4.76), H-6 → L (92.32)
	8	3.0666	H → L+1 (97.77)
	9	3.1625	H-1 → L+1 (98.08)
	10	3.2025	H-10 → L (65.15), H-7 → L (27.87)

Table S7. Natural transition orbitals (NTOs) for (MAMP)$ZnCl_3$.

	n-th	Energy (eV)	Transition configuration (%)
S_n	1	2.4391	H → L (99.77)
	2	2.6110	H-1 → L (99.65)
	3	2.8542	H-2 → L (99.47)
	4	2.9635	H-3 → L (99.00)
	5	3.1348	H → L+1 (99.48)
	6	3.2090	H-4 → L (99.32)
	7	3.3052	H-1 → L+1 (99.09)
	8	3.5616	H-2 → L (2.09), H-2 → L+1 (94.82)
	9	3.6138	H-2 → L (96.62)
	10	3.6733	H-3 → L+1 (97.08)
T_n	1	2.4333	H → L (99.79)
	2	2.6031	H-1 → L (99.35)
	3	2.8439	H-2 → L (98.88)
	4	2.9232	H-3 → L (95.57)
	5	3.1283	H → L+1 (99.56)
	6	3.1685	H-4 → L (97.27)
	7	3.2947	H-1 → L+1 (99.23)
	8	3.5388	H-5 → L (2.31), H-2 → L (88.40), H-2 → L+1 (2.28%)
	9	3.5664	H-2 → L+1 (96.47)
	10	3.6643	H-3 → L+1 (94.11), H-2 → L+1 (2.37)

Table S8. Natural transition orbitals (NTOs) for(MAEP)$ZnCl_3$.

	n-th	Energy (eV)	Transition configuration (%)
S_n	1	2.4519	H → L (99.78)
	2	2.5855	H-1 → L (99.68)
	3	2.8268	H-2 → L (98.7)
	4	2.9811	H → L+1 (99.24)
	5	2.9929	H-3 → L (19.36), H → L+1 (79.93)
	6	3.1205	H-1 → L+1 (98.97)
	7	3.2081	H-4 → L (99.15)
	8	3.3722	H-2 → L+1 (98.4)
	9	3.4738	H → L+2 (99.43)
	10	3.5300	H-3 → L+1 (97.28)
*T*n	1	2.4455	H → L (99.73)
	2	2.5787	H-1 → L (99.54)
	3	2.8109	H-2 → L (97.2)
	4	2.9526	H-3 → L (93.99), H-2 → L (2.18)
	5	2.9872	H-3 → L (79.22), H → L+1 (19.35)
	6	3.1127	H-1 → L+1 (98.74)
	7	3.1683	H-4 → L (95.65)
	8	3.3606	H-2 → L+1 (97.66)
	9	3.4719	H → L+2 (99.39)
	10	3.4975	H-5 → L (91.87), H-3 → L+1 (2.78)

Table S9. Natural transition orbitals (NTOs) for (MAMP)$ZnBr_3$.

	n-th	Energy (eV)	Transition configuration (%)
S_n	1	2.0834	H → L (99.81)
	2	2.2572	H-1 → L (99.70)
	3	2.5055	H-2 → L (99.85)
	4	2.6410	H-3 → L (99.20)
	5	2.7696	H → L+1 (99.39)
	6	2.8663	H-4 → L (99.17)
	7	2.9421	H-1 → L+1 (98.76)
	8	3.2073	H-2 → L+1 (98.83)
	9	3.2328	H-5 → L (95.68), H-2 → L+1 (3.41)
	10	3.3354	H-3 → L+1 (98.81)
T_n	1	2.0782	H → L (99.83)
	2	2.2500	H-1 → L (99.61)
	3	2.4948	H-2 → L (99.75)
	4	2.6123	H-3 → L (97.95)
	5	2.7619	H → L+1 (99.30)
	6	2.8268	H-4 → L (98.28)
	7	2.9289	H-1 → L+1 (99.24)
	8	3.1782	H-5 → L (94.43)
	9	3.2115	H-5 → L (3.27), H-2 → L+1 (96.19)
	10	3.3258	H-3 → L+1 (97.87)

Table S10. Natural transition orbitals (NTOs) for (MAMP)$ZnCl_4$.

	n-th	Energy (eV)	Transition configuration (%)
S_n	1	1.7290	H → L (99.64%)
	2	1.7649	H-1 → L (99.63%)
	3	2.3076	H-4 → L (2.54%), H-3 → L (10.99%), H-2 → L (85.93%)
	4	2.3686	H-3 → L (86.64%), H-2 → L (11.59%)
	5	2.4563	H → L+1 (98.62%)
	6	2.4849	H-5 → L (4.02%), H-4 → L (89.93%)
	7	2.4928	H-1 → L+1 (98.19%)
	8	2.6673	H-5 → L (93.97%), H-4 → L (3.72%)
	9	2.8667	H-6 → L (96.99%)
	10	3.0398	H-4 → L+1 (2.21%), H-3 → L+1 (6.83%), H-2 → L+1 (90.22%)
T_n	1	1.7275	H → L (99.61%)
	2	1.7634	H-1 → L (99.56%)
	3	2.2916	H-4 → L (2.49%), H-3 → L (4.67%), H-2 → L (92.32%)
	4	2.3567	H-3 → L (91.88%), H-2 → L (5.30%)
	5	2.4558	H → L+1 (98.01%)
	6	2.4754	H-5 → L (3.68%), H-4 → L (89.95%), H-3 → L (2.31%)
	7	2.4922	H-1 → L+1 (99.31%)
	8	2.6362	H-5 → L (93.25%), H-4 → L (3.21%)
	9	2.8307	H-6 → L (94.91%)
	10	3.0273	H-7 → L (5.56%), H-3 → L+1 (2.15%), H-2 → L+1 (89.37%)

3. Reference

1. K. Robinson, G. Gibbs and P. Ribbe, Quadratic elongation: a quantitative measure of distortion in coordination polyhedra, *Science*, 1971, **172**, 567-570.